ELSEVIER

Thermochimica Acta 399 (2003) 189–201

thermochimica acta

www.elsevier.com/locate/tca

Errors and correction in complex heat capacity measurements by temperature modulated DSC

Katsuhiko Kanari [a], Takeo Ozawa [b,*]

[a] *Electrotechnical Laboratory, Tsukuba 305-8568, Japan*
[b] *Chiba Institute of Technology, Tsudanuma 275-0016, Japan*

Received 25 March 2002; received in revised form 13 August 2002; accepted 16 August 2002

Abstract

For complex heat capacity measurements, various types of temperature modulated differential scanning calorimetry (tm-DSC) can be used. However, three factors have influence on steady state of tm-DSC and hence cause errors in complex heat capacity measurements. These factors are heat capacities along heat paths in the instrument, temperature distribution within the sample, and thermal contact among the sample, the sample cell and its holder plate. They are theoretically investigated by a set of comprehensive fundamental equations of heat balance based on a common model applicable to all existing types of tm-DSC. For heat paths in the instrument, heat loss to the environment and mutual heat exchange between the sample and the reference material are also taken into accounts, beside the main heat flows from the heat sources to the sample and the reference material. Rigorous and general solutions have been obtained, and useful relations for complex heat capacity measurements have been derived for each type of tm-DSC. Examining the solutions, new insight into tm-DSC is obtained, and errors and their correction are discussed. They are characteristic of tm-DSC types and compared with each other.

Keywords: Temperature modulated DSC; Heat flux DSC; Power compensation DSC; Photo-modulated DSC; Complex heat capacity measurement; Steady state; Error; Correction

1. Introduction

One of remarkable capabilities of temperature modulated differential scanning calorimetry (tm-DSC) is complex heat capacity measurement. Since publication of tm-DSC by Reading and coworkers [1,2], this method has been extensively studied. Thermal contact between the sample cell and its holder plate was pointed out for its influence on the temperature oscillation early in 1971 by Gobrecht et al. [3] and later by Hatta and Muramatsu [4]. The present authors also elucidated that heat capacities along heat paths also have effect on the temperature oscillation [5–9]. These two factors were discussed together in a general theory for all existing types of tm-DSC by using a set of comprehensive fundamental equations of heat balance based on a common model [9]. Later, influence of temperature distribution within the sample (in other word, propagation of temperature wave in the sample) has been theoretically discussed [10–15].

To measure heat capacity in high precision and to detect the imaginary part of heat capacity, an exact theoretical consideration for eliminating the influence of these factors is essentially needed, because these factors cause error. It is also of fundamental importance for sound development of tm-DSC that the potential capability of its complex heat capacity

* Corresponding author.
E-mail address: ozaw.7214@nifty.com (T. Ozawa).

0040-6031/02/$ – see front matter
PII: S0040-6031(02)00463-X

Nomenclature

List of symbols[1]

c^*	the complex specific heat capacity
$C(C^*)$	the heat capacity (the complex heat capacity)
d	the thickness of the sample
t	the time
T	the temperature
P^*	the complex amplitude of the oscillating thermal power input
P_0	the constant (non-oscillating) thermal power input
K	the heat transfer coefficient
x	the vertical coordinate in the sample

Greek symbols

λ	the thermal conductivity
ρ	the density

Subscripts for the temperature T and the power input P[2]

cs	the sample cell
cr	the reference material cell
f	the furnace
fr	the midpoint between the furnace and the reference material
fs	the midpoint between the furnace and the sample
hr	another similar point near the reference material
hs	a point in the heat path for the mutual heat exchange
o	the environment
ps	the sample cell holder plate
pr	the reference material cell holder plate

Subscripts for the heat transfer coefficient K

cr	that between the reference material cell and its holder
cs	the thermal contact between the sample cell and its holder plate
h	the mutual heat exchange
K	the heat paths from the furnace to the sample and the reference material
o	the heat loss to the environment from the cell holder plate through the temperature sensor leads and/or by the purge gas
so	the heat loss from the top surface of the sample by the purge gas

*Subscripts for the heat capacities C and C**

c	the sample cell or the reference material cell
h	the heat path for the mutual heat exchange
K	the heat path between the furnace and the sample or the reference material
p	the cell holder plate

[1] The asterisks mean that the quantities are complex to express the amplitude and the phase difference. The absolute value of P^* is equal to or less than P_0 for each combination, because the sum of P^* and P_0 expresses the thermal power input and it must be not minus but zero or plus.

[2] Subscripts for the power inputs P indicate the points to which the power is supplied.

measurement should be realized on sound physical base.

In this paper, the above three factors influencing complex heat capacity measurements have been taken into accounts together in a general theory for all existing types of tm-DSC. The types of tm-DSC dealt with in this paper are direct temperature modulation either for heat flux DSC (tm-hf-DSC) [5] or power compensation DSC (tm-pc-DSC) [7] and indirect temperature modulation for hf-DSC by modulated light irradiation (photo-modulated DSC; pm-DSC) [8]. The common model and a set of fundamental equations of heat balance in this paper are similar to but a little bit different from those in the previous paper [9]. They have been revised in one point that mathematically the sample is treated not as a point but as a continuum, so that the temperature wave propagation within the sample can be taken into account. In spite of this complicated phenomenon, the mathematical method applied in the previous paper can also be applied to the new fundamental equations, because the situation we are dealing with is a steady state and the solutions for the temperatures at various points can be assumed rigorously. Thus, the mathematical derivation becomes relatively easy, though it is complicated. Because the common

model and comprehensive equations have been used, the results can be applied to all types of tm-DSC, and the comparison among them is feasible. The results and discussion on them are described in this paper.

2. Generalized models

A generalized common model used in this paper covers all existing types of tm-DSC, i.e. tm-pc-DSC, tm-hf-DSC and pm-DSC. In the generalized model, the power is supplied to the sample and the reference material from multiple heat sources; namely the common furnace to the sample and the reference material, the micro-heaters specific to the sample and the reference material, the light sources beneath the cell holder plates, and the light sources above the sample and the reference material [9]. For applying the solutions to each type of the actual apparatus, unnecessary heat sources are eliminated.

In the previous papers [5–9], the instrument and the sample were represented by an equivalent electrical circuit in which the thermal resistance and the heat capacity of the sample, the heat paths etc. are assumed to be concentrated at points. They are represented with discrete electrical resistors and capacitors in an electrical circuit of concentrated constants. As mentioned above, the difference of the new generalized model from the previous models is that the sample is not a point but a continuum, through which the temperature wave is propagating with decrease in the amplitude and shift of the phase angle (a distributed constant circuit). However, the other parts are modeled with the above electrical circuit of concentrated constants, so that the whole equivalent circuit is a mixed circuit of concentrated constants and distributed constants.

Another important factor influencing the temperature oscillation is thermal contacts among the sample, the sample cell and its holder plate. To take this factor into accounts, the cell and the holder are separated in the model and thermal resistance is inserted between them.

The heat flows in various DSC instruments are:

- the main heat flow from the common furnace to the sample and the reference material;
- the heat loss to the environment by purge gas and through the temperature sensor leads;
- the mutual heat exchange between the sample side and the reference material side;
- the heat supply from the micro-heaters and the light sources.

These heat flows are all considered in the following comprehensive fundamental equations of heat balance. The instrument is assumed to be symmetrical; for instance the heat capacities and the heat transfer coefficients in the sample side are the same as those in the reference material side, but an empty cell is used for the reference material in the model.

For describing the temperature wave propagating through the sample, approximations are introduced. Usually, the disc-like sample pan is used, and its diameter is much larger than its thickness, so that it can be approximated as a disc of infinite diameter. Therefore, the lateral temperature distribution is assumed to be negligibly small and there is only the vertical distribution, as described in Appendix A.

Furthermore, the sample cell is made of aluminum or other metal, and its thermal conductivity and thermal diffusivity are both large enough, so that the temperature distribution within the sample cell material is neglected. Thermal contact between the sample and the sample cell is assumed to be good enough and thermal resistance between them is also neglected. It is also assumed that the temperature wave is propagating in the sample cell material without thermal resistance, hence without the amplitude decrement and the phase angle shift. Therefore, the temperature wave is penetrating into the inside of the sample equally from both the bottom and the top (or the lid) of the sample cell. Then the temperature distribution within the sample is symmetrical to its vertical direction and the lateral temperature distribution is assumed negligible. The heat does not flow at the half depth of the sample because of the above vertical symmetry. By replacing the sample thickness, d, by $d/2$, therefore, the solution for this model can be applied to the case that the temperature wave is penetrating into the sample only from the bottom, while the top surface is adiabatic.

Thus the generalized comprehensive models have been made, and they are commonly applicable to all types of tm-DSC. They can be shown in a form of electrical equivalent circuits and it is similar to that shown in the previous paper [9] except the distributed constant circuit for the sample. Following

these generalized model, a set of the fundamental equations have been formulated and solved.

Fundamental equations of heat balance are solved assuming the equations for the temperatures in the steady state, as was done in the previous papers [5–9]. These are quite similar to the previous ones except the temperature wave propagation within the sample, so that the mathematical derivations are described in Appendix A. To derive the equations for the steady state in each type of real tm-DSC, some unnecessary elements should be eliminated from the general solutions.

3. Comprehensive solutions

3.1. Solutions for constant temperature lags

As is described in Appendix A, we have got the general solution for the non-oscillating temperature difference and the non-oscillating power inputs:

$$\Delta C' = \frac{\Delta P_0 + \Delta P_{p0} + \Delta B_p K}{\beta - \beta'_{ps}} \tag{1}$$

where $\Delta C'$, ΔP_0, ΔP_{p0}, ΔB_p, K and β are difference in the real heat capacity (at zero frequency) between the sample and the reference material, that in the light power input from above, that in the power input from below and that in the constant temperature lag, sum of the heat transfer coefficients in the instrument, as defined in Appendix A, and the heating rate, respectively, and the term, $\beta - \beta'_{ps}$, expresses the heating rate of the sample cell holder plate.

For hf-DSC where are no additional power inputs, $\Delta P_0 = \Delta P_{p0} = 0$, so that

$$\Delta C' = \frac{\Delta B_p K}{\beta - \beta'_{ps}} \tag{2}$$

This equation expresses the principle for conventional heat capacity measurement by hf-DSC. Similarly for pc-DSC where the temperature difference is controlled to be zero, $\Delta B_p = \Delta P_0 = 0$:

$$\Delta C' = \frac{\Delta P_{p0}}{\beta - \beta'_{ps}} \tag{3}$$

The above equation has been used also for conventional heat capacity measurement by pc-DSC.

It should be noted that the temperature distribution within the sample is not involved in these equations, but actually temperature gradient exists in the sample for heat flow from the sample cell to the inside of the sample. In the above mathematical treatment, this temperature gradient has no effect on the measurements, because the heat capacity is assumed to be independent on the temperature. In actual conventional measurements, the heat capacity measured is that averaged for the temperature distribution within the sample.

3.2. Solutions for oscillating temperatures

For differences in the oscillating temperature and the oscillating power inputs, we have the following solution:

$$F^*_{exp}\Delta C^*_s = \frac{\Delta P^*_p + \Delta P^*_{sr} - F^*_{app}\Delta A^*_p}{A^*_{ps}} \tag{4}$$

where F^*_{exp} and F^*_{app} are both correction factors described in Appendix A, and ΔC^*_s, ΔP^*_p, ΔP^*_{sr}, ΔA^*_p and A^*_{ps} are difference in the complex heat capacity between the sample and the reference material (including the sample cell), that in the complex amplitude of the modulated power input from below, that from above (some correction factors are included; see Appendix A), the complex amplitude of the oscillating temperature difference between the sample and the reference material, and the complex amplitude of the oscillating temperature of the sample cell holder plate, respectively. It should be noted that ΔC^*_s is naturally dependent on the frequency.

The factors, F^*_{exp} and F^*_{app}, are very complicated as given in the Appendix A. The former factor, F^*_{exp}, is dependent on the experimental conditions, such as the frequency, the sample thickness, the sample thermal conductivity, the heat capacity per unit volume of the sample and the thermal contact between the cell and its holder plate. Thus F^*_{exp} should be called the experimental correction factor.

On the other hand, F^*_{app} is characteristic of the apparatus dependent on the heat transfer coefficients and the heat capacities of the heat paths in the instrument, though it also depends on the frequency. Therefore, it is the instrumental correction factor, which does not change run by run for the same frequency measurement.

Similar to the above equations for conventional heat capacity measurements by DSC, the next equation is obtained for tm-hf-DSC.

$$F^*_{\mathrm{exp}}\Delta C^*_{\mathrm{s}} = -\frac{F^*_{\mathrm{app}}\Delta A^*_{\mathrm{p}}}{A^*_{\mathrm{ps}}} \tag{5}$$

because $\Delta P^*_{\mathrm{p}} = \Delta P^*_{\mathrm{sr}} = 0$.

For tm-pc-DSC, where $\Delta P^*_{\mathrm{sr}} = \Delta A^*_{\mathrm{p}} = 0$,

$$F^*_{\mathrm{exp}}\Delta C^*_{\mathrm{s}} = \frac{\Delta P^*_{\mathrm{p}}}{A^*_{\mathrm{ps}}} \tag{6}$$

For pm-DSC irradiated from below,

$$F^*_{\mathrm{exp}}\Delta C^*_{\mathrm{s}} = \frac{\Delta P^*_{\mathrm{p}} - F^*_{\mathrm{app}}\Delta A^*_{\mathrm{p}}}{A^*_{\mathrm{ps}}} \tag{7}$$

because $P^*_{\mathrm{p}} \neq 0$ and $\Delta P^*_{\mathrm{sr}} = 0$.

Similar but somewhat different equation is applied to pm-DSC irradiated from above.

$$F^*_{\mathrm{exp}}\Delta C^*_{\mathrm{s}} = \frac{\Delta P^*_{\mathrm{sr}} - F^*_{\mathrm{app}}\Delta A^*_{\mathrm{p}}}{A^*_{\mathrm{ps}}} \tag{8}$$

In this equation, it should be noted that ΔP^*_{sr} is not the difference in the power input by light irradiation but the corrected difference, for which the thermal contact effect is taken into accounts (Appendix A).

4. Discussion

It becomes clear from the above solutions that the oscillatory quantity directly measured by any type of tm-DSC is not the complex heat capacity nor its difference between the sample and the reference material, ΔC^*_{s}, but uncorrected apparent complex heat capacity difference or effective complex heat capacity difference, $F^*_{\mathrm{exp}}\Delta C^*_{\mathrm{s}}$, which is a quantity effective for influencing the temperature oscillation and is corresponding to thermal inertia against the temperature oscillation. Because the experimental correction factor, F^*_{exp}, is complicated and dependent on the various factors, the correction is very difficult. In addition to this, for hf-DSC, including pm-DSC, the instrumental correction factor, F^*_{app}, is additionally needed to correct the temperature difference oscillation due to the temperature wave propagation (heat flow) in the apparatus.

To measure the complex heat capacity, these two corrections should be done. The correction factor, F^*_{app}, is first considered. It is for the amplitude decrement and the phase shift by the instrument, and this is needed only for hf-DSC including pm-DSC. (The amplitude decrement and the phase shift due to electronics in the instruments occur in all types of tm-DSC [3].) These effects including the electronics effect can be detected and measured in a region, where the imaginary part of the sample heat capacity is zero, with the experimental conditions of negligible effect of the thermal contact and the negligible effect of temperature distribution within the sample, using the sample of known heat capacity. Thus we can estimate F^*_{app} by this conditions.

To elucidate the effect of the other correction factor, F^*_{exp}, it has been calculated as a function of the influencing factors, i.e. the sample thickness, the thermal contacts, the sample thermophysical properties and the frequency. The calculation has been made for polymer and ceramics, because their thermal diffusivity is low, and it is easily imagined that the correction is needed for these samples even if the sample is thin. The thermophysical properties used in the calculation are listed in Table 1. The samples are corresponding to polymer (polystyrene) and ceramics (silica glass and titania), which are not powder but nonporous plates. The values in Table 1 are those for zero frequency, and the imaginary parts of heat capacity are zero. Therefore, the ratio of the imaginary part of the heat capacity to the real part, $\tan\delta$ is hypothetically assumed and indicated in the figures of the calculated results.

The thermal contact assumed in this calculation is one-hundredth of perfect contact. The thermal conductance for the perfect contact is assumed to equal to that of aluminum of 0.6 μm thickness, and this contact (113.1 W/K) seems good contact. For these

Table 1
Density, heat capacity and thermal conductivity used in calculation

Sample	ρ (kg/m^3)	c_s (kJ/kg K)	λ (W/mK)
Polystyrene	1050	1.23	0.135
Silica glass	2200	0.692	1.38
Titania	4175	0.692	8.4
Air	1.3	1.1	0.02

The data in this table are cited from *Thermophysical Properties Handbook* edited by the Japan Society of Thermophysical Properties, Yokendo, Tokyo, 1990.

parameters the correction factor, F^*_{exp}, was calculated by using Eq. (A.31).

Taking the complicated calculation of F^*_{exp} into account, the realistic way for us to measure accurately the complex heat capacity is to find a region where the correction for the sample thickness is not needed because of negligible effect. The errors of uncorrected data are calculated for this purpose, and the errors are defined as follows; for the real part, $|C'_s(1-F'_{exp})/C^*_{s0}|$ and for the imaginary part, $|C''_s(1-F''_{exp})/C^*_{s0}|$, respectively, where $||$ means the absolute value and

$$C^*_{s0} = \sqrt{C'^2_s + C''^2_s} \tag{9}$$

$$F^*_{exp} = F'_{exp} - iF''_{exp} \tag{10}$$

The results are shown in Figs. 1 and 2. From these figures we can learn the maximum allowable sample thickness in relation to the frequency (or the period, p) for the measurement of required accuracy without the correction. For polymers (see Fig. 1), if we wish to measure the complex heat capacity within 0.5 % inaccuracy, the thickness of the sample should be less than 0.25 mm for the period larger than 100 s. For ceramics the restriction is not so tight as seen in Fig. 2, and it is about 1mm. Naturally, the restriction is much loose for plate metal sample. In relation to this, it is interesting to note that larger apparent so-called non-reversing heat flow (i.e. the out-of-phase heat flow) is experimentally observed for α-alumina powder than for α-alumina plate [16]. This fact clearly shows the effect of sample thermal diffusivity on the complex heat capacity measurements. Powdered sample and porous sample are not suitable for this measurement.

It is very interesting to present the calculation results in a way such as the Cole–Cole plot [3,11]. It is the plot of the imaginary part of the apparent heat capacity, i.e. $C''_s F''_{exp}$ versus its real part, $C'_s F'_{exp}$. The results are shown in Fig. 3. As is seen in this figure, the calculated data of the real and imaginary parts of apparent heat capacity for these three samples are roughly on arched curves like the Cole–Cole plot for dielectrics. The real and imaginary parts of correct heat capacity are located at the right end point. The influencing factors, i.e. the sample thickness and the period, have the similar effect of shifting the data to the left side on the arched curve. The deviation is the larger for the thicker sample and the higher frequency. (Note that the complex heat capacity has the frequency dependence in its nature, so that the effect of the sample thickness is different from the frequency effect.) Low thermal diffusivity has the same effect, as is clear in comparison between silica glass and titania. Dividing the apparent values by C^*_{s0} (normalization), we have very interesting results, as seen in Fig. 4. All

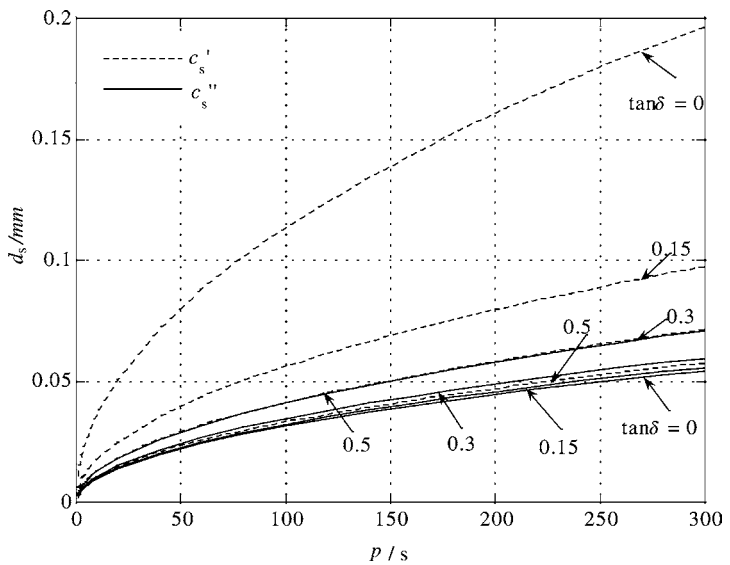

Fig. 1. Allowable thickness and period of polystyrene sample for indicated hypothetical tan δ.

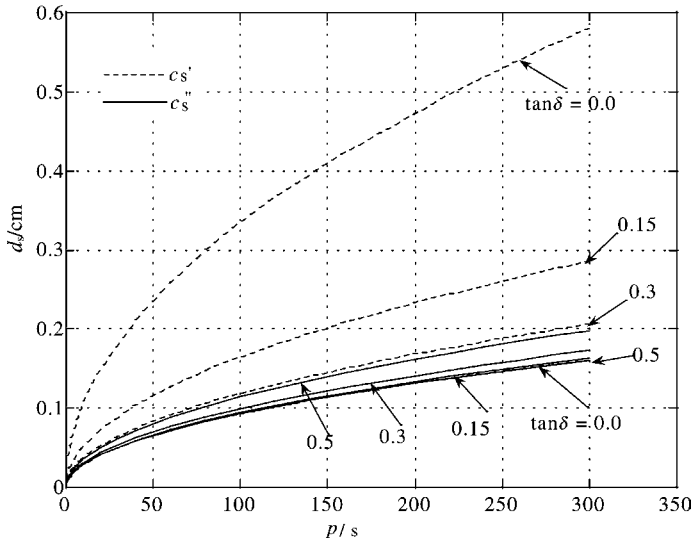

Fig. 2. Allowable thickness and period of silica glass sample for indicated hypothetical tan δ.

data for the three different samples are on an arched curve.

By changing tan δ arbitrarily, we have different arched curves as in Figs. 5 and 6. In these cases, the correct values are located at the right ends. Again interesting results are obtained by normalization, as seen in Fig. 7. However, it is not sure that the similar results can be obtained for other values of C_s^* and

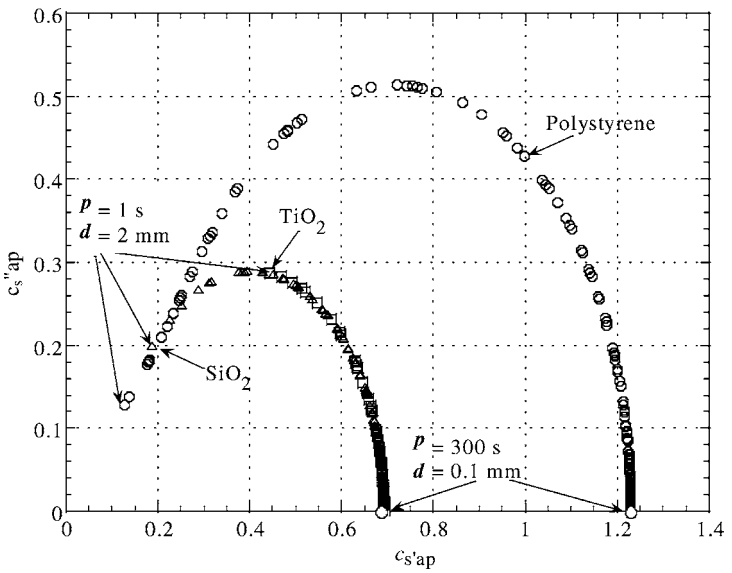

Fig. 3. Cole–Cole plots of imaginary part of apparent complex heat capacity vs. real part for polystyrene, silica glass and titania for tan $\delta = 0$. The period and thickness are indicated in the figure, and the others are for the data obtained under other conditions. The thickness and the period are changed from 0.1 to 2 mm and from 300 to 1 s, respectively. The symbols, ○, △ and □ are for polystyrene, silica glass and titania, respectively.

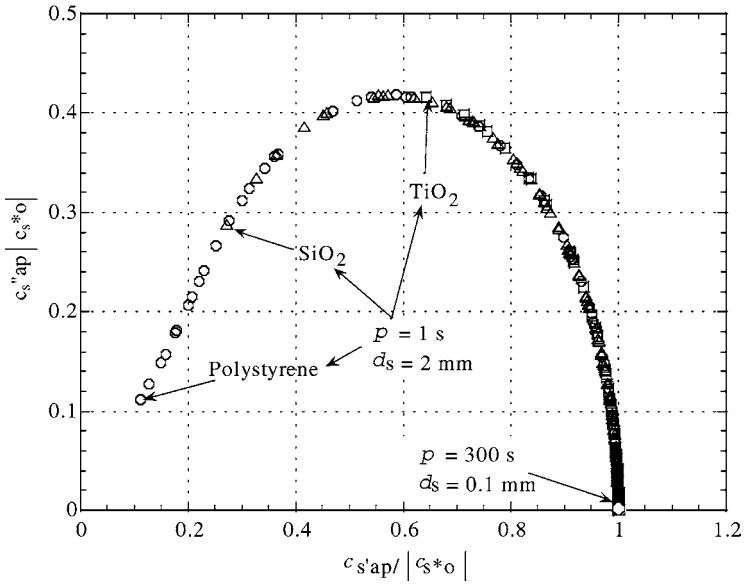

Fig. 4. Normalized Cole–Cole plots of imaginary part of apparent complex heat capacity vs. real part for polystyrene, silica glass and titania for $\tan\delta = 0$. The period and thickness are indicated in the figure, and the others are for the data obtained under other conditions. The thickness and the period are changed from 0.1 to 2 mm and from 300 to 1 s, respectively. The symbols, ○, △ and □ are for polystyrene, silica glass and titania, respectively.

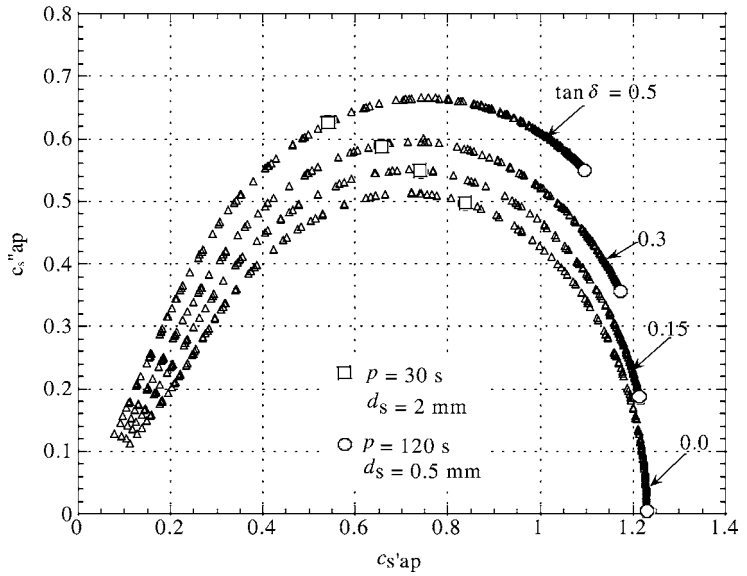

Fig. 5. Cole–Cole plots of imaginary part of apparent complex heat capacity vs. real part for polystyrene for different hypothetical $\tan\delta$. The period and thickness are indicated in the figure, and the others are for the data obtained under other conditions. The thickness and the period are changed from 0.1 to 2 mm and from 300 to 1 s, respectively. The symbols are indicated in the figure.

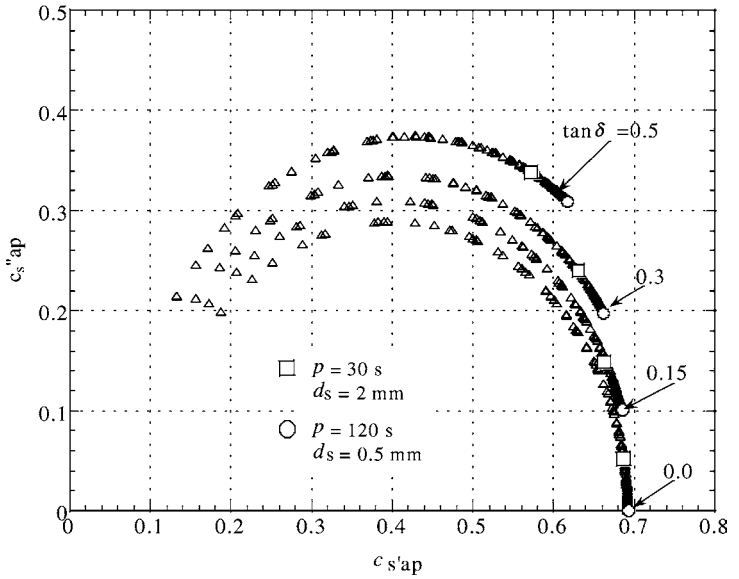

Fig. 6. Cole–Cole plots of imaginary part of apparent complex heat capacity vs. real part for silica glass for different hypothetical tan δ. The period and thickness are indicated in the figure, and the others are for the data obtained under other conditions. The thickness and the period are changed from 0.1 to 2 mm and from 300 to 1 s, respectively. The symbols are indicated in the figure.

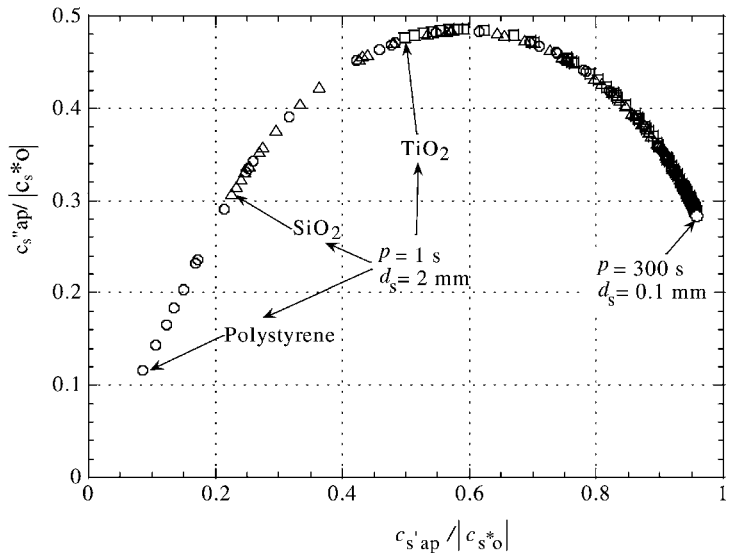

Fig. 7. Normalized Cole–Cole plots of imaginary part of apparent complex heat capacity vs. real part for polystyrene, silica glass and titania for hypothetical values of tan $\delta = 0.3$. The period and thickness are indicated in the figure, and the others are for the data obtained under other conditions. The thickness and the period are changed from 0.1 to 2 mm and from 300 to 1 s, respectively. The symbols, ○, △ and □ are for polystyrene, silica glass and titania, respectively.

other thermal diffusivity, because the results in Figs. 4 and 7 are obtained as numerical solutions.

For the effect of thermal contact among the sample, the sample cell and the cell holder, similar calculation was made. When the results are plotted in the Cole–Cole plot, different arched curves are obtained for different thermal contact, and a larger arched curve is observed for lower thermal contact, but the correct value at the right end is common.

We should consider the other correction for the thermal contact effect. One of the ways for this purpose is to use heat resistant grease or liquid metal to keep thermal contact good enough. Because this effect appears as imaginary temperature difference oscillation in a region where the imaginary part of the sample heat capacity is zero, it can be detected as this imaginary oscillation. Methods for this correction have been discussed elsewhere [9], and they can be applied to the data, for which the effect of the temperature distribution can be neglected by using the sample of the appropriate thickness.

In order to consider these error factors in the measurements, it is very helpful to plot the estimated imaginary part of complex heat capacity versus the estimated real part of complex heat capacity, such as in Figs. 3–7. It was done by Toda et al. for the measured data [17]. The data located at the right end of the arched curve should be the most accurate. Furthermore, when the data does not shift for a certain range of the sample thickness, the sample thickness can be in a region where the effect of the temperature wave propagation is negligible.

5. Conclusion

1. For all existing types of tm-DSC the errors by the sample thickness (due to the temperature wave propagation) and the thermal contact among the sample, the sample cell and its holder plate are theoretically considered with that due to the heat flow in the instrument. The general solution is obtained, in which the correction factor for the former error, the experimental error, is separately involved with that for the instrumental error due to the heat flow within the instrument.
2. Therefore, the correction for the experimental error can be done separately with the instrumental error.
3. The instrumental error correction factor can be obtained by the measurement with the sample of known heat capacity.
4. Because the experimental error is dependent complicatedly on the sample thickness, the thermal contact, the sample thermophysical properties and the frequency, it is realistic to find the region in which the error is less than allowable error. The region was found by the calculation of specific cases. Then the correction can be made for the thermal contact separately.
5. The plot of the imaginary part of measured apparent heat capacity versus its real part, such as the Cole–Cole plot, is very helpful to see these error effects.

Appendix A.

A.1. Fundamental equations of heat balance

First, a set of comprehensive fundamental equations is formulated for the models, as follows. For the concentrated constants circuit, the following equations are applied as in the previous paper [9]:

$$C_{\mathrm{K}}\frac{\mathrm{d}T_{\mathrm{fs}}}{\mathrm{d}t} = 2K_{\mathrm{K}}(T_{\mathrm{f}} - T_{\mathrm{fs}}) + 2K_{\mathrm{K}}(T_{\mathrm{ps}} - T_{\mathrm{fs}}) \quad \text{(A.1)}$$

$$C_{\mathrm{c}}\frac{\mathrm{d}T_{\mathrm{cs}}}{\mathrm{d}t} = K_{\mathrm{cs}}(T_{\mathrm{ps}} - T_{\mathrm{cs}}) + 2\lambda_{\mathrm{s}}S\left(\frac{\partial T_{\mathrm{s}}(x,t)}{\partial x}\right)_{x=0} + P^{*}_{\mathrm{cs}}\exp(\mathrm{i}\omega t) + P_{\mathrm{cs0}} \quad \text{(A.2)}$$

$$C_{\mathrm{p}}\frac{\mathrm{d}T_{\mathrm{ps}}}{\mathrm{d}t} = 2K_{\mathrm{K}}(T_{\mathrm{fs}} - T_{\mathrm{ps}}) + 3K_{\mathrm{h}}(T_{\mathrm{hs}} - T_{\mathrm{ps}}) + K_{\mathrm{o}}(T_{\mathrm{o}} - T_{\mathrm{ps}}) + K_{\mathrm{cs}}(T_{\mathrm{cs}} - T_{\mathrm{ps}}) + P^{*}_{\mathrm{ps}}\exp(\mathrm{i}\omega t) + P_{\mathrm{ps0}} \quad \text{(A.3)}$$

$$C_{\mathrm{h}}\frac{\mathrm{d}T_{\mathrm{hs}}}{\mathrm{d}t} = 3K_{\mathrm{h}}(T_{\mathrm{ps}} - T_{\mathrm{hs}}) + 3K_{\mathrm{h}}(T_{\mathrm{hr}} - T_{\mathrm{hs}}) \quad \text{(A.4)}$$

$$C_{\mathrm{h}}\frac{\mathrm{d}T_{\mathrm{hr}}}{\mathrm{d}t} = 3K_{\mathrm{h}}(T_{\mathrm{pr}} - T_{\mathrm{hr}}) + 3K_{\mathrm{h}}(T_{\mathrm{hs}} - T_{\mathrm{hr}}) \quad \text{(A.5)}$$

$$C_{\mathrm{p}}\frac{\mathrm{d}T_{\mathrm{pr}}}{\mathrm{d}t} = 2K_{\mathrm{K}}(T_{\mathrm{fr}} - T_{\mathrm{pr}}) + 3K_{\mathrm{h}}(T_{\mathrm{hr}} - T_{\mathrm{pr}}) + K_{\mathrm{o}}(T_{\mathrm{o}} - T_{\mathrm{pr}}) + K_{\mathrm{cr}}(T_{\mathrm{cr}} - T_{\mathrm{pr}}) + P^{*}_{\mathrm{pr}}\exp(\mathrm{i}\omega t) + P_{\mathrm{pr0}} \quad \text{(A.6)}$$

$$C_c \frac{dT_{cr}}{dt} = 2K_{cr}(T_{pr} - T_{cr}) + P^*_{cr} \exp(i\omega t) + P_{cr0} \quad (A.7)$$

and

$$C_K \frac{dT_{fr}}{dt} = 2K_K(T_f - T_{fr}) + 2K_K(T_{pr} - T_{fr}) \quad (A.8)$$

A.2. Temperatures distribution in the sample

For the distributed constants circuit expressing the sample temperature distribution,

$$\frac{\lambda_s \partial^2 T_s(x,t)}{\partial^2 x} = \frac{c^*_s \rho_s \partial T_s}{\partial t} \quad (A.9)$$

with boundary conditions:

$$T_s(0,t) = T_{cs} \quad \text{at } x = 0 \text{ and } x = d \quad (A.10)$$

$$\frac{\lambda_s \partial T_s(x,t)}{\partial x} = 0 \quad \text{at } x = \frac{d}{2} \quad (A.11)$$

The asterisks for C^*_s means that the heat capacity is assumed to be complex heat capacities consisting of the real and the imaginary parts as follows:

$$C^*_s = C'_s - iC''_s \quad (A.12)$$

where i, C^*_s, C'_s and C''_s are the units of imaginary numbers, the frequency-dependent complex sample heat capacity, its real part and its imaginary part, respectively.

A.3. Derivation of comprehensive solutions

In the steady state, any temperature, T_i, changes at a fixed frequency, an amplitude and a constant underlying heating rate, so that

$$T_i = T_b + A^*_i \exp(i\omega t) + \beta t - \beta'_i t - B_i \quad (A.13)$$

where T_b, A^*_i, ω, β, β'_i and B_i are the initial temperature, the complex amplitude expressing the amplitude and the phase angle, the angular frequency, the programmed underlying heating rate, the decrease of the underlying heating rate due to the heat loss to the environment, and the constant temperature lag, respectively. The subscript i is one of the subscripts for the temperatures (f, fs, s, r, cs, cr, ps, pr, fr, hs or hr). In this equation,

$$\exp(i\omega t) = \cos(\omega t) + i\sin(\omega t) \quad \text{[Euler equation]} \quad (A.14)$$

and

$$A^* \exp(i\omega t) = A'\cos(\omega t) + A''\sin(\omega t) + iA''\cos(\omega t) + iA'\sin(\omega t) \quad (A.15)$$

where

$$A^* = A' + iA'' \quad (A.16)$$

For the temperature within the sample, the next equation can be applied similarly,

$$T_s(x,t) = T_b + A^*_i(x)\exp(i\omega t) + \beta(x)t - \beta'_i(x)t - B_i(x) \quad (A.17)$$

In this equation, $T_s(x, t)$, $A^*_i(x)$, $\beta(x)$, $\beta'_i(x)$ and $B_i(x)$ are functions of the vertical coordinate.

In these equations related with the temperatures, only the real part has physical meaning and the imaginary part should be neglected. This is the same for the temperatures and the temperature differences below.

The comprehensive general solutions are derived from the fundamental equations of heat balance, and the derivation is described below.

First of all, Eq. (A.13) for i = cs and Eq. (A.17) are introduced into Eq. (A.9) with the boundary conditions, Eqs. (A.10) and (A.11), and the coefficients in these equations are compared as was done in the previous paper [6]. Thus, we have the next equation for $T_s(x, t)$.

$$T_s(x,t) = T_o + (\beta - \beta_{cs})t + \left(\frac{\cosh\{\varepsilon^*(x-d)\}}{\cosh(\varepsilon^* d)}\right) A^*_{cs} \exp(i\omega t) - \left\{\frac{c^*_s \rho_s (\beta - \beta_{cs})}{\lambda_s}\right\}\left(dx - \frac{x^2}{2}\right) + \beta_{cs} \quad (A.18)$$

where

$$\varepsilon^* = \varepsilon' + i\varepsilon'' \quad (A.19)$$

$$\varepsilon' = \pm\sqrt{\frac{\omega c'_s \rho_s f_1}{2\lambda_s}} \quad (A.20)$$

$$\varepsilon'' = \pm\sqrt{\frac{\omega c'_s \rho_s f_2}{2\lambda_s}} \quad (A.21)$$

$$f_1 = \sqrt{1 + \tan\delta^2} + \tan\delta \quad (A.22)$$

$$f_1 = \sqrt{1 + \tan\delta^2} - \tan\delta \tag{A.23}$$

$$\tan\delta = \frac{c_s''}{c_s'} \tag{A.24}$$

Between the symmetrical points in the instrument, the following equation holds:

$$\Delta T_k = T_i - T_j = \Delta A_k^* \exp(\mathrm{i}\omega t) - \Delta\beta_k' t - \Delta B_k \tag{A.25}$$

where Δ means the difference of the quantity and the subscripts i and j are the symmetrical points (fs versus fr, ps versus pr and hs versus hr), the subscript k meaning the difference between them (f for fs − fr, p for ps − pr and h for hs − hr). Similarly, for the symmetrical points we have the next fundamental equations of the heat balance.

$$C_\mathrm{K}\frac{\mathrm{d}\Delta T_\mathrm{f}}{\mathrm{d}t} = 2K_\mathrm{K}\Delta T_\mathrm{p} - 4K_\mathrm{K}\Delta T_\mathrm{f} \tag{A.26}$$

$$C_\mathrm{h}\frac{\mathrm{d}\Delta T_\mathrm{h}}{\mathrm{d}t} = 3K_\mathrm{h}\Delta T_\mathrm{p} - 9K_\mathrm{h}\Delta T_\mathrm{h} \tag{A.27}$$

and

$$\begin{aligned} C_\mathrm{p}\frac{\mathrm{d}\Delta T_\mathrm{p}}{\mathrm{d}t} &= 2K_\mathrm{K}\Delta T_\mathrm{f} + 3K_\mathrm{h}\Delta T_\mathrm{h} \\ &\quad - (2K_\mathrm{K} + 3K_\mathrm{h} + K_\mathrm{o})\Delta T_\mathrm{p} \\ &\quad + \{K_\mathrm{ps}(T_\mathrm{cs} - T_\mathrm{ps}) - K_\mathrm{pr}(T_\mathrm{cr} - T_\mathrm{pr})\} \\ &\quad + \Delta P_\mathrm{p}^* \exp(\mathrm{i}\omega t) + \Delta P_\mathrm{p0} \end{aligned} \tag{A.28}$$

where

$$\Delta P_\mathrm{p0} = P_\mathrm{ps0} - P_\mathrm{pr0} \tag{A.29}$$

and

$$\Delta P_\mathrm{p}^* = P_\mathrm{ps}^* - P_\mathrm{pr}^* \tag{A.30}$$

Introducing Eqs. (A.18) and (A.25) in Eqs. (A.26)–(A.28), we can get the final equations we are deriving, as was done in the previous paper [5]. They are the comprehensive solution for constant temperature lags (Eq. (2)), where K equals to $K_\mathrm{K} + 2K_\mathrm{h} + K_\mathrm{o}$ and that for the oscillating temperatures (Eq. (5)). In the latter, the following three relations occur:

$$F_\mathrm{exp}^*\Delta C_\mathrm{s}^* = \frac{\mathrm{i}\omega C_\mathrm{c} + \sqrt{\omega C_\mathrm{s}' K_\mathrm{s}}G^*}{1 + \mathrm{i}\omega\tau_\mathrm{cs} + \sqrt{\omega C_\mathrm{s}' K_\mathrm{s}}(G^*/K_\mathrm{ps})} - \frac{\mathrm{i}\omega C_\mathrm{c}}{\mathrm{i}\omega\tau_\mathrm{cr}} \tag{A.31}$$

$$\Delta P_\mathrm{sr}^* = \frac{P_\mathrm{cs}^*}{1 + \mathrm{i}\omega\tau_\mathrm{cs} + \sqrt{\omega C_\mathrm{s}' K_\mathrm{s}}(G^*/K_\mathrm{ps})} - \frac{P_\mathrm{cr}^*}{1 + \mathrm{i}\omega\tau_\mathrm{cr}} \tag{A.32}$$

and

$$F_\mathrm{app}^* = S_1 + \mathrm{i}S_2 \tag{A.33}$$

where

$$\begin{aligned} S_1 &= (2K_\mathrm{K} + 3K_\mathrm{h} + K_\mathrm{o}) - \frac{K_\mathrm{K}}{(1 + \omega^2\tau K^2)} \\ &\quad - \frac{K_\mathrm{h}}{(1 + \omega^2\tau_\mathrm{h}^2)} + \frac{2\omega^2 C_\mathrm{c}\tau_\mathrm{cr}^2}{(1 + \omega^2\tau_\mathrm{cr}^2)} \end{aligned} \tag{A.34}$$

$$\begin{aligned} \frac{S_2}{\omega} &= \frac{C_\mathrm{K}}{4(1 + \omega^2\tau K^2)} + \frac{C_\mathrm{h}}{9(1 + \omega^2\tau_\mathrm{h}^2)} \\ &\quad + \frac{C_\mathrm{c}}{(1 + \omega^2\tau_\mathrm{cr}^2)} + C_\mathrm{p} \end{aligned} \tag{A.35}$$

$$\tau_\mathrm{K} = \frac{C_\mathrm{K}}{4K_\mathrm{K}} \tag{A.36}$$

$$\tau_\mathrm{h} = \frac{C_\mathrm{K}}{9K_\mathrm{h}} \tag{A.37}$$

$$\tau_\mathrm{cs} = \frac{C_\mathrm{c}}{4K_\mathrm{cs}} \tag{A.38}$$

$$\tau_\mathrm{cr} = \frac{C_\mathrm{c}}{4K_\mathrm{cr}} \tag{A.39}$$

$$K_\mathrm{s} = \lambda_\mathrm{s}\frac{S}{d} \tag{A.40}$$

$$C_\mathrm{s}' = 2Sdc_\mathrm{s}'\rho_\mathrm{s} \tag{A.41}$$

and

$$G^* = \tanh(\varepsilon^* d)(\sqrt{f_1} + \sqrt{f_2}) \tag{A.42}$$

References

[1] M. Reading, D. Elliott, V.L. Hill, J. Therm. Anal. 40 (1993) 949.
[2] P.S. Gill, S.R. Sauerbrunn, M. Reading, J. Therm. Anal. 40 (1993) 931.
[3] H. Gobrecht, K. Hamann, G. Willers, J. Phys. E: Sci. Instrum. 4 (1971) 21.
[4] I. Hatta, S. Muramatsu, Jpn. J. Appl. Phys. 35 (1996) L858.
[5] T. Ozawa, Pure Appl. Chem. 69 (1997) 2315.
[6] T. Ozawa, K. Kanari, Thermochim. Acta 288 (1996) 39.

[7] T. Ozawa, K. Kanari, J. Thermal Anal. Calor. 56 (1999) 691.
[8] T. Ozawa, K. Kanari, Thermochim. Acta 338 (1999) 7.
[9] T. Ozawa, K. Kanari, J. Thermal Anal. Calor. 59 (2000) 257.
[10] I. Hatta, A.A. Minakov, Thermochim. Acta 330 (1999) 39.
[11] M. Merzlykov, C. Schick, Thermochim. Acta 330 (1999) 65.
[12] F.U. Buehler, J.C. Seferis, Thermochim. Acta 334 (1999) 49.
[13] E.-Y. Ding, R.-S. Cheng, Y.-H. Huang, Thermochim. Acta 336 (1999) 1.
[14] E.-Y. Ding, R.-S. Cheng, Thermochim. Acta 378 (2001) 51.
[15] S.L. Simon, Thermochim. Acta 374 (2001) 55.
[16] H. Higashiyama, T. Ozawa, unpublished data.
[17] A. Toda, T. Arita, C. Tomita, M. Hikosaka, Polymer 41 (2000) 8941.